
Controlling Continuous Relaxation for Combinatorial Optimization

Yuma Ichikawa

Fujitsu Limited, University of Tokyo

{ichikawa.yuma@fujitsu.com, ichikawa-yuma1@g.ecc.u-tokyo.ac.jp }

Abstract

Recent advancements in combinatorial optimization (CO) problems emphasize the potential of graph neural networks (GNNs). The physics-inspired GNN (PI-GNN) solver, which finds approximate solutions through unsupervised learning, has attracted significant attention for large-scale CO problems. Nevertheless, there has been limited discussion on the performance of the PI-GNN solver for CO problems on relatively dense graphs where the performance of greedy algorithms worsens. In addition, since the PI-GNN solver employs a relaxation strategy, an artificial transformation from the continuous space back to the original discrete space is necessary after learning, potentially undermining the robustness of the solutions. This paper numerically demonstrates that the PI-GNN solver can be trapped in a local solution, where all variables are zero, in the early stage of learning for CO problems on the dense graphs. Then, we address these problems by controlling the continuity and discreteness of relaxed variables while avoiding the local solution: (i) introducing a new penalty term that controls the continuity and discreteness of the relaxed variables and eliminates the local solution; (ii) proposing a new continuous relaxation annealing (CRA) strategy. This new annealing first prioritizes continuous solutions and intensifies exploration by leveraging the continuity while avoiding the local solution and then schedules the penalty term for prioritizing a discrete solution until the relaxed variables are almost discrete values, which eliminates the need for an artificial transformation from the continuous to the original discrete space. Empirically, better results are obtained for CO problems on the dense graphs, where the PI-GNN solver struggles to find reasonable solutions, and for those on relatively sparse graphs. Furthermore, the computational time scaling is identical to that of the PI-GNN solver.

1 INTRODUCTION

Combinatorial optimization (CO) problems is a fundamental problem in many critical real-world applications, including transportation logistics, scheduling, network design, and energy management [Glover et al., 2019, Kochenberger et al., 2014, Anthony et al., 2017, Papadimitriou and Steiglitz, 1998, Korte et al., 2011]. Specifically, CO problems aim to find the minimum or maximum value of an objective function from a discrete space of candidate solutions. While some problems can be solved efficiently by problem-specific methods, many practical problems can be more complex and large-scale, requiring a broadly applicable and scalable method rather than methods specific to individual problems. Therefore, such solvers have been proposed based on statistical mechanics, such as adiabatic quantum computation [Albash and Lidar, 2018] and Fujitsu Digital Annealer [Aramon et al., 2019]. However, these methods still suffer scalability limitation and struggle to treat complex many-body interactions.

Recently, motivated by developments in machine learning, machine-learning-assisted solvers have been developed. In particular, graph neural networks (GNNs) [Gilmer et al., 2017, Scarselli et al., 2008] are known to be useful for CO problems on graphs since GNNs have an inductive bias that automatically learns a useful graph representation by repeatedly aggregating the features of neighboring nodes. Especially among them, physics-inspired graph neural network (PI-GNN) solver [Schuetz et al., 2022a,b] is getting significant attention. Specifically, the PI-GNN solver is based on a continuous relaxation strategy: parameterizing relaxed variables by GNNs and then solving a CO problem as an unsupervised node classification task using an objective function that is differentiable with respect to the GNN parameters. The PI-GNN solver performs on par or outperforms existing solvers, with the ability to scale to CO problems with millions of variables and directly treats any multi-body interaction and Potts variables.

Note that the PI-GNN solver has inherent ambiguity for the transformation from relaxed continuous variables to original discrete variables after learning, potentially undermining the robustness of the solutions. In fact, while linear relaxation returns an integral optimal solution on bipartite graphs by Huffman-Kruskal theorem [Hoffman and Kruskal, 2010], it is known to have half-integrality: every extreme point for relaxed problems is half-integral, that is, all elements are 0, $1/2$, or 1 [Nemhauser and Trotter Jr, 1974]. In addition, there needs to be more discussion on the performance of the PI-GNN solver for CO problems on relatively dense graphs where the performance of greedy algorithms worsens. As pointed out in [Angelini and Ricci-Tersenghi, 2023], these issues are vital for investigating the performance of the PI-GNN solver and can be a crucial bottleneck for real-world problems.

In this paper, we numerically investigate the performance of the PI-GNN solver for CO problems on relatively dense random regular graphs (RRGs). This experiment reveals that, as the graph is denser, the PI-GNN solver is trapped in a local solution where all relaxed variables are zero during the early stages of learning. This phenomenon can be a significant bottleneck when deploying the PI-GNN solver in practical applications. Then, we remedy these problems by continuous relaxation annealing (CRA) which controls the continuity and discreteness of relaxed variables and eliminates the local solution. CRA is based on (i) a new penalty term to control the continuity and discreteness of relaxed variables and a parameter, denoted as γ , to adjust the strength of the penalty term; if gamma γ is smaller, the relaxed variable tends to favor continuous solutions, whereas if gamma γ is larger, the relaxed variable prefers discrete solutions, (ii) a newly proposed annealing method gradually increasing γ until the relaxed variables are almost discrete values, which eliminates the need of an artificial transformation from the continuous to the original discrete space after learning. Empirically, the CRA-PI-GNN solver can find reasonable solutions to CO problems on the dense graphs, where the PI-GNN solver fails, with nearly the same computational time scaling. Moreover, for sparser graph problems, the results surpass those of the PI-GNN solver with the computational time.

Contributions The main contributions of the paper are as follows:

- It is numerically demonstrated that the PI-GNN solver gets trapped in a local minimum, where all relaxed variables are zero, for CO problems on relatively dense graphs, where the performance of greedy algorithms deteriorates, then failing to find a reasonable solution.
- We propose a new penalty term designed to control both the continuity and discreteness of relaxed variables and eliminate the local solution. The penalty term is scheduled from a state favoring continuous space to one favoring discrete space and then automatically transforms relaxed variables from continuous to discrete space.
- Numerically, the proposed CRA method can find better solutions even for both CO problems on the dense graphs, where the PI-GNN solver cannot address, and sparse graphs faster than the PI-GNN solver. In addition, our method automatically outputs an almost discrete solution by the annealing.
- Numerical experiments indicate that the computational time scaling of the proposed method is on par with that of the PI-GNN solver.

2 BACKGROUND

2.1 Combinatorial Optimization and QUBO

CO problems aim to find optimal values from a finite but huge candidate set of solutions. However, in almost practical CO problems, finding an exact solution for a sufficiently large problem is impossible because the candidate set of solutions grows exponentially as the number of variables increases. Therefore, problem-specific algorithms to find approximate solutions have been developed. In contrast to the direction, approaches integrating NP-hard CO problems have also been developed recently. In particular, quadratic unconstrained binary optimization (QUBO) can encode a variety of NP-hard CO problems [Glover et al., 2019, Kochenberger et al., 2014, Anthony et al., 2017, Lucas, 2014, Glover et al., 2018], which is known to be able to encode many NP-complete and NP-hard problems, including Kerp’s 21 NP-complete problems [Lucas, 2014]. Specifically, QUBO formulates the CO problems by the following cost function $\mathcal{H}(\cdot; Q) : \mathbb{R}^N \rightarrow \mathbb{R}$:

$$\mathcal{H}_{\text{QUBO}}(\mathbf{x}; Q) = \mathbf{x}^\top Q \mathbf{x} = \sum_{ij} x_i Q_{ij} x_j, \quad (1)$$

where $\mathbf{x} = (x_1, \dots, x_N) \in \{0, 1\}^N$ is a binary vector of fixed length $N > 0$ and the matrix $Q \in \mathbb{R}^{N \times N}$ is a square matrix that encodes the CO problems. The global minimum can be determined over all possible binary variables, which can quickly become infeasible as the number of variables grows. Despite these challenges, the ability to formulate a wide range of optimization problems as QUBO makes it an indispensable tool in tackling CO problems. Hereafter, we briefly describe specific CO problems, their corresponding QUBOs used in our numerical experiments, and their underlying theoretical background.

Maximum Independent Set The MIS problem is an NP-hard CO problem [Karp, 2010] that has various practical applications [Hale, 1980, Boginski et al., 2005] and benchmark problems in previous studies [Schuetz et al., 2022a]. The MIS problem is defined as follows. Given an undirected graph $\mathcal{G}(\mathcal{V}, \mathcal{E})$ where \mathcal{V} is the set of nodes with cardinality $|\mathcal{V}| = N$ and $\mathcal{E} \subseteq \mathcal{V} \times \mathcal{V}$ is the set of edges, an independent set (IS) $\mathcal{I} \subseteq \mathcal{V}$ is defined as a subset of nodes that are not directly connected to any two nodes. The MIS problem then requires finding the largest IS denoted as \mathcal{I}^* . The independent set density is defined as the density of the IS, i.e., $\rho = |\mathcal{I}|/|\mathcal{V}|$. To consider the QUBO corresponding to MIS problems, a binary variable x_i is assigned to each node $i \in \mathcal{V}$, where the variable x_i indicates whether the node is included in the IS or not; while $x_i = 1$ indicates that the node is included in the IS, $x_i = 0$ indicates that the node is not included in the IS. The MIS problem is identical to maximizing the number of nodes assigned 1 while ensuring that the nodes assigned 1 are not adjacent to each other. Thus, the MIS problem can be formulated as

$$\mathcal{H}_{\text{MIS}}(\mathbf{x}; P) = - \sum_{i \in \mathcal{V}} x_i + P \sum_{(i,j) \in \mathcal{E}} x_i x_j, \quad (2)$$

where the first term tries to maximize the number of nodes assigned 1, and the second term penalizes nodes assigned 1 being adjacent to each other. Here, the parameter $P > 0$ controls the strength of the constraint, typically set as $P = 2$ [Djidjev et al., 2018]. In the subsequent numerical analysis, we focus on the MIS problems on random d -regular graphs (d -RRGs), where every node is connected to exactly d other nodes. There are some theoretical results for the MIS problems. First, for every d , a specific value ρ_d^* , which depends only on the degree d , exists such that the independent set density $|\mathcal{I}^*|/|\mathcal{V}|$ converges to ρ_d^* with a high probability as N approaches infinity [Bayati et al., 2010]. Second, a statistical mechanical analysis provides the typical maximum independent set density ρ_d^{Theory} , plotted in Fig. 2, and clarify that for $d > 16$, the solution space of \mathcal{I} undergoes a clustering transition, which is associated with hardness in sampling [Barbier et al., 2013] because the clustering is likely to create relevant barriers that affect any algorithm searching for the MIS \mathcal{I}^* . Lastly, the hardness is supported by analytical results in large d limit, indicating that while the maximum independent set density is known to have density $\rho_{d \rightarrow \infty}^* = 2 \log(d)/d$, there is no known algorithm that finds an independent set density exceeding $\rho_{d \rightarrow \infty}^{\text{alg}} = \log(d)/d$ [Coja-Oghlan and Efthymiou, 2015].

Maximum Cut The MaxCut problem is also one of the fundamental NP-hard optimization problems [Karp, 2010] with practical applications [Alidaee et al., 1994, Neven et al., 2008, Deza and Laurent,

1994]. The MaxCut problem is defined as follows. Given an undirected graph $\mathcal{G} = (\mathcal{V}, \mathcal{E})$ with cardinality $|\mathcal{V}| = N$, a cut set $\mathcal{C} \in \mathcal{E}$ is defined as a subset of the edge set between node sets partitioning $\{\mathcal{V}_1, \mathcal{V}_2 \mid \mathcal{V}_1 \cup \mathcal{V}_2 = \mathcal{V}, \mathcal{V}_1 \cap \mathcal{V}_2 = \emptyset\}$. Then, the objective of the MaxCut problem is to find the maximum cut set denoted as \mathcal{C}^* . The cut ratio is defined as the ratio of the cardinality of the cut set, $|\mathcal{C}|$, to the cardinality of the vertex set, $|\mathcal{V}|$, i.e., $\nu = |\mathcal{C}|/|\mathcal{V}|$. To formulate the MaxCut problem as QUBO, a binary variable is assigned to each node $i \in \mathcal{V}$, where $x_i = 1$ indicates that node i belongs to \mathcal{V}_1 and $x_i = 0$ indicate node belongs to \mathcal{V}_2 . It can be confirmed that $x_i + x_j - 2x_i x_j = 1$ holds if the edge (i, j) is part of the cut set, and is equal to 0 otherwise. Thus, the MaxCut problem can be formulated as

$$\mathcal{H}_{\text{MaxCut}}(\mathbf{x}; A) = \sum_{i < j} A_{ij}(2x_i x_j - x_i - x_j) \quad (3)$$

where A_{ij} is the adjacency matrix with $A_{ij} = 0$ if an edge (i, j) does not exist and $A_{ij} > 0$ if the edge connects. This paper also focuses on the MaxCut problems on d -RRGs, where several theoretical results have been established. Specifically, for each d , the maximum cut ratio is given by $\nu_d^* \approx d/4 + P_* \sqrt{d/4} + \mathcal{O}(\sqrt{d})$ where $P_* = 0.7632 \dots$ with a high probability as N approaches infinity [Parisi, 1980, Dembo et al., 2017]. Thus, we take $\nu_d^{\text{UB}} = d/4 + P_* \sqrt{d/4}$ as an upper bound for the maximum cut ratio in the large N limit.

2.2 Graph Neural Networks

A graph neural network (GNN) [Gilmer et al., 2017, Scarselli et al., 2008] is a specialized neural network for representation learning of graph-structured data. GNNs learn a vectorial representation of each node through two steps. (i) Aggregate step: This step employs a permutation-invariant function to generate an aggregated node feature. (ii) Combine step: Subsequently, the aggregated node feature is passed through a trainable layer to generate a node embedding, known as ‘message passing’ or ‘readout phase.’ Formally, for given graph $\mathcal{G} = (\mathcal{V}, \mathcal{E})$, where each node feature $\mathbf{h}_v^0 \in \mathbb{R}^{N^0}$ is attached to each node $v \in \mathcal{V}$, the GNN iteratively updates the following two steps. First, the aggregate step at each k -th layer is defined by

$$\mathbf{a}_v^k = \text{Aggregate}_\theta^k(\{\mathbf{h}_u^{k-1}, \forall u \in \mathcal{N}_v\}), \quad (4)$$

where the neighborhood of $v \in \mathcal{V}$ is denoted as $\mathcal{N}_v = \{u \in \mathcal{V} \mid (v, u) \in \mathcal{E}\}$, \mathbf{h}_u^{k-1} is the node feature of neighborhood, and \mathbf{a}_v^k is the aggregated node feature of the neighborhood. Second, the combined step at each k -th layer is defined by

$$\mathbf{h}_v^k = \text{Combine}_\theta^k(\mathbf{h}_v^{k-1}, \mathbf{a}_v^k), \quad (5)$$

where $\mathbf{h}_v^k \in \mathbb{R}^{N^k}$ denotes the node representation at k -th layer. The total number of layers, K , and the intermediate vector dimension, N^k , are empirically determined hyperparameters. Although numerous implementations for GNN architectures have been proposed, the most basic and widely used GNN architecture is a graph convolutional network (GCN) [Scarselli et al., 2008] given by

$$\mathbf{h}_v^k = \sigma \left(W^k \sum_{u \in \mathcal{N}(v)} \frac{\mathbf{h}_u^{k-1}}{|\mathcal{N}(v)|} + B^k \mathbf{h}_v^{k-1} \right), \quad (6)$$

where W^k and B^k are trainable parameters, $|\mathcal{N}(v)|$ serves as normalization factor, and $\sigma : \mathbb{R}^{N^k} \rightarrow \mathbb{R}^{N^k}$ is some component-wise nonlinear activation function such as sigmoid or ReLU function.

2.3 Physics-Inspired Graph Neural Networks

Continuous relaxation is a strategy that reformulates an original CO problem into a continuous optimization problem by converting discrete variables into continuous ones instead. In a QUBO problem, one of the continuous relaxations can be represented as

$$\hat{\mathcal{H}}_{\text{QUBO}}(\mathbf{p}; Q) = \mathbf{p}^\top Q \mathbf{p} = \sum_{ij} p_i Q_{ij} p_j, \quad (7)$$

where $\mathbf{p} = (p_1, \dots, p_N) \in [0, 1]^N$ is a set of relaxed continuous variables, that is, each binary variable $x_i \in \{0, 1\}$ is relaxed to a continuous variable $p_i \in [0, 1]$, which can be interpreted as

binary class probabilities associated with the node. Generally, continuous relaxation can simplify CO problems by transforming a discrete and potentially non-convex problem into a continuous and often convex one. This transformation is more amenable to mathematical and computational techniques since the gradient information of the cost function is typically available. However, continuous relaxation poses two challenges. First, there is a potential disagreement between the optimal solutions of a discrete original CO problem and relaxed continuous ones since the relaxation can expand the solution space and then often results in a deviation from the original discrete binary values. Second, the relaxed solution obtained from the relaxed CO problem must be transformed into the original discrete space. As a result, the results may vary based on the chosen transformation method.

PI-GNN solvers, as proposed by Schuetz et al. [2022a,b], solve CO problems as a unsupervised node classification task, without the need for any labelled data. Specifically, the PI-GNN solver parameterize the relaxed continuous variables through GNNs:

$$\hat{\mathcal{H}}_{\text{QUBO}}(\theta, \phi; Q) = \mathbf{p}_\theta^\top(\mathbf{h}_{\phi, \mathcal{G}}^0) Q \mathbf{p}_\theta(\mathbf{h}_{\phi, \mathcal{G}}^0) = \sum_{ij} p_{\theta, i}(\mathbf{h}_{\phi, \mathcal{G}}^0) Q_{ij} p_{\theta, j}(\mathbf{h}_{\phi, \mathcal{G}}^0), \quad (8)$$

where the input consists of node embedding vectors, denoted as $\mathbf{h}_{\phi, \mathcal{G}}^0 \in \mathbb{R}^{N^0}$, $N^0 \in \mathbb{N}$ where ϕ is a trainable parameter, and the relaxed continuous vector is denoted as $\mathbf{p}_\theta : \mathbb{R}^{N^0} \rightarrow [0, 1]^{N^0}$ where θ is the trainable parameters of the GNNs. Note that the relaxation-based PI-GNN solver can handle many-body interactions beyond just two-body interactions and binary variables [Schuetz et al., 2022a,b]. The PI-GNN solver can be trained using a gradient-based algorithm to minimize Eq (8) since the cost function is generally differentiable with respect to the GNN model parameters. After training the GNN, the continuous solution is converted into discrete variables simply by $x_i = \text{int}(p_{\theta, i}(\mathbf{h}_{\mathcal{G}}^0))$ for all $i = 1, \dots, N$. It is important to emphasize that this machine-learning parameterizing approach is not restricted to GNNs and can be extended to other deep-learning models. A more sophisticated architecture will be left for future research.

3 PI-GNN SOLVER: HOW CAN IT FAIL?

This section shows the potential limitations of the PI-GNN solver when applied to more complex CO problems where the performance of greedy algorithms worsens. As Angelini and Ricci-Tersenghi [2023] emphasized, It is crucial to assess the PI-GNN solver on such complex CO problems, including MIS problems on higher-degree RRGs, as discussed in Sec. 2.1. In response to [Angelini and Ricci-Tersenghi, 2023], [Schuetz et al., 2023] argues that, although the MIS problems on higher-degree RRGs are academically intriguing, these problems deviate from typical real-world problems, inherently limiting their applicability in real-world scenarios. However, if the PI-GNN solver is entirely non-functional for such MIS problems, it could become a potential bottleneck for more practical and relatively dense problems, making it challenging to employ the PI-GNN solver confidently. Additionally, comparisons with existing solvers and theoretical results on such MIS problems are indispensable to ensure the performance of the PI-GNN solver.

Therefore, we conduct numerical experiments of the PI-GNN solver on the MIS and MaxCut problems on higher-degree RRGs. To guarantee the utmost experimental impartiality, we adhered to the original settings of the GNN-Solver [Schuetz et al., 2022b]; see Sec. 5.1 for detailed experimental configurations. Fig. 1 (Top) shows the approximate solutions of the PI-GNN solver as a function of degree d for MIS and MaxCut problems with varying system size N . The results indicate that finding any independent and cut sets becomes infeasible as the graph becomes denser. Moreover, to clarify the origin of the failure, we examined the dynamics of the cost function for MIS problems with $N = 10000$, particularly focusing on the instance when degree $d = 5$ and $d = 20$ as depicted in Fig. 1 (Bottom). For the instance on $d = 5$, the dynamics goes over the plateau of $\mathcal{H}_{\text{QUBO}}(\theta, \phi; Q) = 0$ with $\mathbf{p}_\theta = (0, \dots, 0) \in \mathbb{R}^N$, investigated in the histogram, and then find a reasonable approximate solution comparable to [Schuetz et al., 2022a]. Conversely, for the instance on $d = 20$, as emphasized in [Angelini and Ricci-Tersenghi, 2023], the dynamics stays on the plateau of $\mathcal{H}_{\text{QUBO}}(\theta, \phi; Q) = 0$ with $\mathbf{p}_\theta = (0, \dots, 0) \in \mathbb{R}^N$ and then can not find any independent set. Note that both results indicate that the relaxed variable tends to be $\mathbf{p}_\theta^*(\mathbf{h}_{\phi, \mathcal{G}}) = (0, \dots, 0) \in \mathbb{R}^N$ during the early stages of learning, which slows down the learning process.

Interpreting this phenomenon, we assume that the representation capacity of the GNN is sufficiently large and then consider optimizing $\mathcal{H}_{\text{QUBO}}(\theta, \phi; Q)$ as a variational optimization problem with

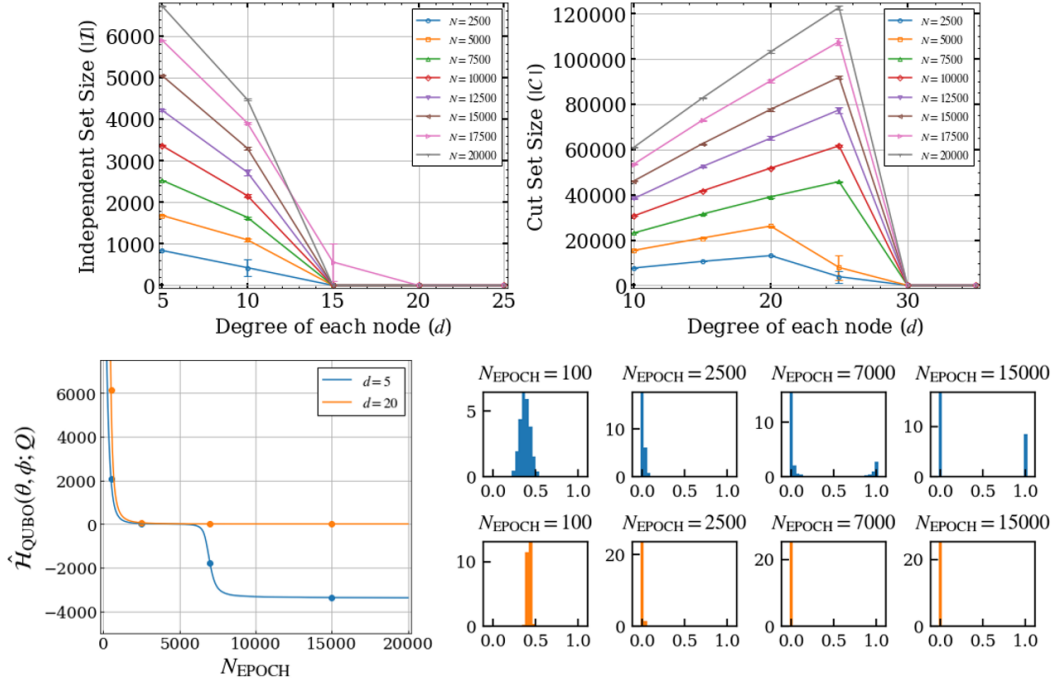


Figure 1: The top graph depicts the independent set density for MIS problems (Left) and cut ratio for MaxCut problems (Right) as a function of degree d using the PI-GNN solver with varying system size N . Each data point represents the average result of five different graph instances, with error bars indicating the standard deviation of those results. The bottom graph shows the cost as a function of the number of parameter updates, N_{EPOCH} , for $N = 10000$ MIS problems on 5-RRG and 20-RRG. The histogram represents the relaxed vector distribution with varying parameter update N_{EPOCH} . Each point in the bottom-left plot is linked to the corresponding bottom-right histogram.

respect to \mathbf{p} . For this case, $\mathbf{p}^* = (0, \dots, 0) \in \mathbb{R}^N$ meets the first-order variational optimality conditions, i.e., $\delta \hat{\mathcal{H}}_{\text{QUBO}}(\mathbf{p}; Q) / \delta \mathbf{p} |_{\mathbf{p}=\mathbf{p}^*} = (0, \dots, 0) \in \mathbb{R}^N$. This implies a potential reason for absorption into $\mathbf{p}^*(\mathbf{h}_{\phi, \mathcal{G}}) = (0, \dots, 0) \in \mathbb{R}^N$. However, this examination does not reveal the conditions for convergence to the fixed point \mathbf{p}^* during the early stage of learning and the condition for escaping from the fixed point \mathbf{p}^* . Therefore, a more in-depth theoretical understanding through the stability analysis of the fixed point remains a topic for future research.

4 METHODS

4.1 Penalty Term to Control the Degree of Discreteness and Continuity

We propose a penalty term to control the discreteness and continuity of relaxed variables. Specifically, the penalty term is introduced to the relaxed QUBO problems as follows:

$$\hat{\mathcal{H}}_{\text{QUBO}}(\mathbf{p}; Q, \gamma) = \sum_{ij} p_i Q_{ij} p_j + \gamma \sum_i (1 - (2p_i - 1)^2), \quad (9)$$

where $\gamma \in \mathbb{R}$ indicate a tuning parameter. For a negative value of γ , i.e., $\gamma < 0$, the relaxed variables prefer the continuous space. On the other hand, for a positive value of γ , i.e., $\gamma > 0$, the relaxed variables prefer discrete space. In addition, the penalty term eliminates the fixed point $\mathbf{p}^* = (0, \dots, 0)$ as discussed in Sec. 3, which leads to avoiding convergence to the fixed point \mathbf{p}^* . While the penalty term in Eq. (9) is the L^2 norm-based penalty term for simplicity, a more sophisticated penalty term mirroring the behavior when changing γ , e.g., L^p norm-based penalty, will be left for future research. Besides, for the Potts variables appearing in the coloring problem, one can achieve a similar effect by adding a constraint term to control continuity and discreteness, as well as another penalty term

ensuring only a single discrete value is taken. For the PI-GNN solver, the penalty term is introduced as follows:

$$\hat{\mathcal{H}}_{\text{QUBO}}(\theta, \phi; Q, \gamma) = \sum_{ij} p_{\theta,i}(\mathbf{h}_{\phi,\mathcal{G}}^0) Q_{ij} p_{\theta,j}(\mathbf{h}_{\phi,\mathcal{G}}^0) + \gamma \sum_i (1 - (2p_{\theta,i}(\mathbf{h}_{\phi,\mathcal{G}}^0) - 1)^2). \quad (10)$$

By setting the gamma γ sufficiently large, the relaxed variables approach almost discrete variables. As a result, the artificial transformation to an original discrete space is not necessary and then obtain robust results.

4.2 Annealing the Penalty Term

As discussed in Sec. 3, the PI-GNN solver exhibits the long plateau at $\mathbf{p}^* = (0, \dots, 0) \in \mathbb{R}^N$ and struggles to escape from the plateau for CO problems on higher-degree RRGs. To address the problem, we propose a annealing strategy that gradually annealing the penalty term in Eq. (10) to control the balance between discreteness and continuity of the relaxed variables. Specifically, set a negative gamma, i.e., $\gamma < 0$, to leverage the properties that eliminates the fixed point $\mathbf{p}^* = (0, \dots, 0)$ and facilitate extensive exploration by relaxed continuous space during the early stage of learning. Then, gradually increase the gamma γ every update of the trainable parameters denoted as 1 epoch until the penalty term is almost zero, which indicates that all variables are almost discrete. While various annealing schedule can be considered, this paper use the following straightforward scheduling:

$$\gamma(N_{\text{EPOCH}} + 1) \leftarrow \gamma(N_{\text{EPOCH}}) + \varepsilon, \quad (11)$$

where the scheduling rate $\varepsilon \in \mathbb{R}$ is a small constant value and N_{epoch} is the number of updates of the trainable parameter during learning. In the subsequent section, we refer to the PI-GNN using the annealing as the continuous relaxation annealing PI-GNN (CRA-PI-GNN). Note that two additional hyperparameters are introduced: the initial scheduling value $\gamma(0)$ and the scheduling rate ε . Our numerical experiment suggests that better solutions can be obtained when the initial scheduling value, $\gamma(0)$ has a smaller negative value and the scheduling rate ε is smaller; see Appendix A.2 for an additional ablation study for these hyperparameters.

4.3 Monitoring Penalty Term for Early Stopping

The PI-GNN solver, due to the continuous relaxation, often yields solutions that take continuous values, such as 1/2. The continuous output can raise an arbitrariness for the transformation from a continuous to an original discrete space. As a result, the solution can be greatly different depending on the chosen transformation. In the worst-case scenario, an inappropriate transformation can yield solutions that deviate from the original feasible space and violate constraints. To address this problem, we suggest a method that not only monitors the cost function but also the penalty term in Eq. (1), stopping the annealing when the penalty term approaches zero. This method ensures more stable results when transforming from the relaxed continuous variables to the original discrete variables.

5 EXPERIMENT

Our experiments investigate the following questions: (1) Is the CRA-PI-GNN solver capable of finding reasonable solutions even for MIS and MaxCut problems on higher-degree-RRGs ? (2) How does the computational time scaling for CRA-PI-GNN ? (3) Can the CRA-PI-GNN solver find solutions comparable to the Markov chain Monte Carlo (MCMC)-based solver and better than greedy algorithms ?

Sec. 5.1 provides our experimental configuration. Sec. 5.2 compares the results of the CRA-PI-GNN solver with that of the original PI-GNN solver. Sec. 5.3 discusses the computational time scaling of the CRA-PI-GNN solver and also compares the results with the MCMC-based solver and greedy algorithm (GA).

5.1 Configuration

The main objective of our numerical experiments is to compare the CRA-PI-GNN solver with the PI-GNN solver. Thus, we take the same setup described in [Schuetz et al., 2022a, 2023] where a simple two-layer GCN and GraphSAGE [Hamilton et al., 2017] architecture with PyTorch GraphConv

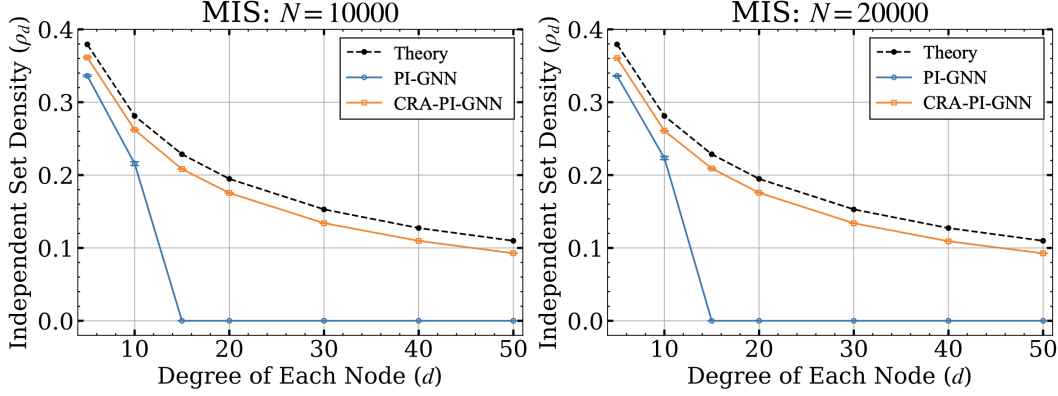


Figure 2: Independent set density of the MIS problem on d -RRG using the PI-GNN and CRA-PI-GNN solver. (Left) the results for graphs of $N = 10000$ nodes. (Right) the results for $N = 20000$ nodes. Each data point illustrates the average results from five different graph instances, with error bars indicating the standard deviation of the results. Various colors correspond to the solvers used, and the dashed lines represent the theoretical results from a statistical mechanical analysis [Barbier et al., 2013].

and GraphSage. The first convolutional layer takes N^0 -dimensional node embedding vectors, $\mathbf{h}_{\phi, \mathcal{G}}^0$, as input, yielding N^1 -dimensional feature vectors $\mathbf{h}_{\phi, \mathcal{G}}^1$. Subsequently, the ReLU function is used as a component-wise nonlinear transformation. The second convolutional layer takes the N^1 -dimensional feature vector, $\mathbf{h}_{\phi, \mathcal{G}}^1$, as input, producing a N^2 -dimensional vector $\mathbf{h}_{\phi, \mathcal{G}}^2$. Finally, a sigmoid function is applied to N^2 -dimensional vector $\mathbf{h}_{\phi, \mathcal{G}}^2$ and then the output is the relaxed approximate solution $\mathbf{p}_\theta \in [0, 1]^N$. As in [Schuetz et al., 2022a], we set $N^0 = \text{int}(\sqrt{N})$, $N^1 = \text{int}(N^0/2)$ and $N^2 = 1$ for both GCN and GraphSAGE. GNNs are initialized with five different random seeds for a single instance because the results depend on the initial values of the trainable parameters and then choose only the best solution. The GNNs are implemented with the Deep Graph Library [Wang et al., 2019]. We use Adam [Kingma and Ba, 2014] as the optimization solver, set the learning rate at $\beta = 10^{-4}$ and train the GNN for up to $\sim 10^5$ epochs, with an early stopping, detailed in Sec. 4.3 set to absolute tolerance of 10^{-5} and patience of 10^3 . Lastly, we set the initial scheduling value $\gamma(0)$ and scheduling rate ε as $\gamma(0) = -20$ and $\varepsilon = 10^{-3}$ for the CRA-PI-GNN solver, respectively. Note that these values are not optimal; refining them can lead the CRA-PI-GNN solver to find a better approximate solutions; see Appendix A.2 for an ablation study regarding these hyperparameters.

5.2 Can CRA-PI-GNN Solver Find a Better Solution on Denser Graphs?

We first numerically compared the solutions of the PI-GNN solver and the CRA-PI-GNN solver with GCV for the MIS and MaxCut problems on d -RRG. A detailed discussion on the computational time scaling of the CRA-PI-GNN solver will be provided in the subsequent section.

Maximum Independent Set Problem. Fig. 2 shows the independent set density as a function of degree d obtained by both the PI-GNN and CRA-PI-GNN solver in comparison to the theoretical results [Barbier et al., 2013]. Setting $P = 2$, we observed very few violated nodes, as in [Schuetz et al., 2022a]. The figure demonstrates that the PI-GNN solver faces problem in finding an independent set for degree $d \geq 15$. However, the CRA-PI-GNN solver can find reasonable approximate solutions even as the degree d increases, even as degree d increases. Even for smaller degrees, specifically $d < 15$, the CRA-PI-GNN solver also outperforms the PI-GNN solver. As a result, the CRA-PI-GNN solver exhibited the ability to find larger independent sets than the PI-GNN solver across all degrees d , and the solution is relatively close to theoretical results. Furthermore, the CRA-PI-GNN solver eliminates the local solution where all variables are zero, allowing the CRA-PI-GNN solver to achieve a better solution with fewer training iterations, N_{EPOCH} than the PI-GNN solver; see Appendix A.1 for the more detailed explanation and dynamics of the cost function. Note that, even when using the

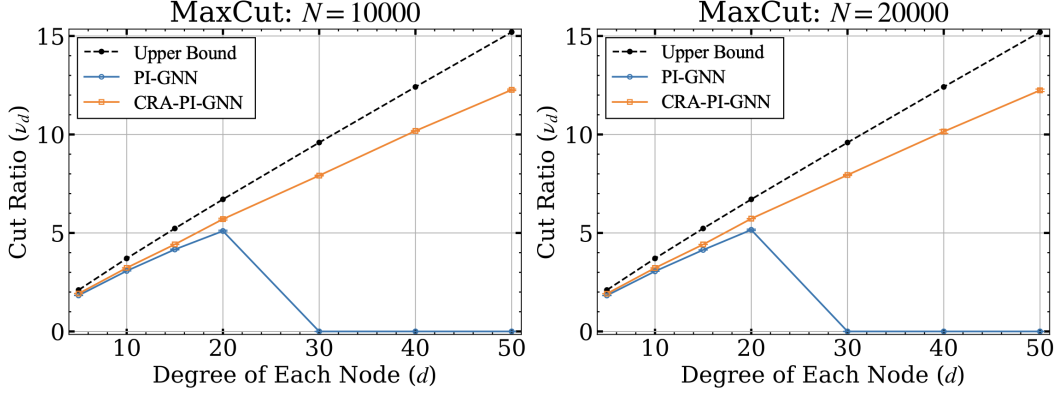


Figure 3: Cut ratio of the MaxCut problem on d -RRG as a function of the degree d using the PI-GNN and CRA-PI-GNN solver. (Left) the results for $N = 1000$ bits. (Right) the results for $N = 2000$ bits. Each data points represent the average results over five different graph instances, with error bars indicating the standard deviations of the results. The different colors represents the solvers employed, and the dashed lines represents the theoretical upper bounds γ_d^{UB} .

PI-GNN solver with the GraphSAGE proposed in the [Schuetz et al., 2023], finding an independent set becomes challenging for larger degrees.

Maximum Cut Problem. Fig. 3 shows the cut ratio as a function of degree d obtained by both the PI-GNN and CRA-PI-GNN solvers in comparison to the theoretical upper bound [Parisi, 1980, Dembo et al., 2017]. The results are similar to the observation of the MIS problems. While the PI-GNN also struggles to find a cut set on $d > 20$, the CRA-PI-GNN solver can find a reasonable approximate solution as the degree of the graph increases. In addition, the CRA-PI-GNN solver can find a better solution even for lower degree, specifically $d \leq 20$, RRG. As a result, the performance of CRA-PI-GNN also consistently surpasses that of the PI-GNN solver across all degree d -RRG.

5.3 Comparison with the Solution Obtained by MCMC-Based Solver and Run Time Scaling

In this section, we compare the solutions obtained from the CRA-PI-GNN solver with those obtained from a solver based on Markov chain Monte Carlo (MCMC) and theoretical results for MIS problem on 100-RRG, as emphasized by [Angelini and Ricci-Tersenghi, 2023]. In addition, we discuss the computational time scaling of the CRA-PI-GNN solver.

The left panel of Fig. 4 shows the independent set density as a function of the number of nodes N obtained by the CRA-PI-GNN, PI-GNN, MCMC-based solvers in temperature denoted as βPT and a greedy algorithm denoted as GA, and theoretical result [Barbier et al., 2013] denoted as Replica; refer to [Angelini and Ricci-Tersenghi, 2019] for a detailed explanation and parameter configurations of βPT and GA. As pointed out in [Schuetz et al., 2023], the figure indicates that the CRA-PI-GNN solver using GraphSAGE provides better results than that using GCV. However, while the CRA-PI-GNN solver using GraphSAGE provides better solutions than GA, it was found to be unable to achieve solutions comparable to βPT . By carefully selecting hyperparameters, one can approach the results of βPT , but never surpass it. However, given that performance varies significantly with network structure, as seen in the differences between GCV and SAGE, identifying a GNN closer to betaPT presents an intriguing future work.

The right panel of Fig. 4, the CRA-PI-GNN solver demonstrates, for large 100-RRG graphs with $N \simeq 10^4$, a moderate super-linear scaling of the total computational time as $\sim N^{1.4}$ for GCN and $\sim N^{1.7}$ for GraphSAGE, almost identical to that of the PI-GNN solver [Schuetz et al., 2022a].

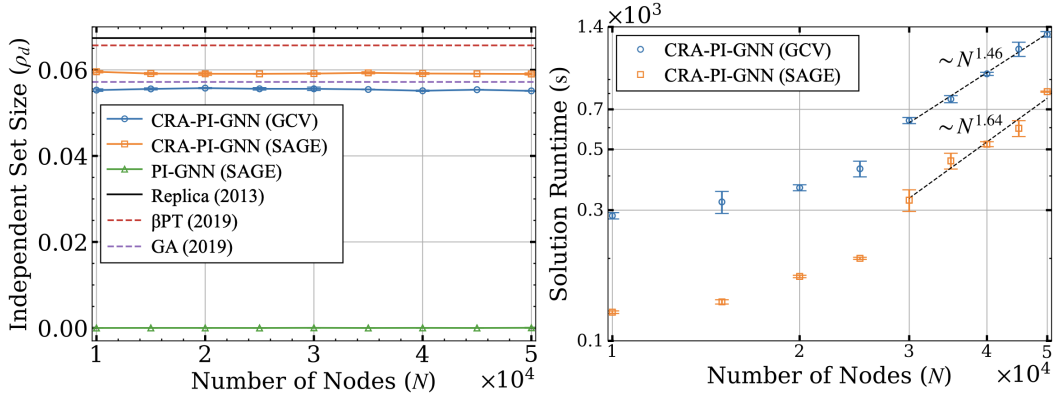


Figure 4: (Left) Independent set density of the MIS problem on 100-RRG with varying the number of nodes N by the CRA-PI-GNN solver, employing both GCN and GraphSage architectures, compared with PI-GNN solver [Schuetz et al., 2022b], the MCMC-based and GA-based solvers [Angelini and Ricci-Tersenghi, 2019], and theoretical results [Barbier et al., 2013]. Each data points represents the average results from five different graph instances. (Right) computational run time in seconds of the CRA-PI-GNN solvers with GraphSage and Conv architectures on 100-RRG with varying the number of nodes N . Error bars represent standard deviations of the results

6 RELATED WORK

Recently, CO solvers using machine learning have attracted significant attention. In particular, unsupervised learning techniques are gaining interest since, unlike supervised learning methods, they can directly solve CO problems without the past solution dataset. This section describes CO solvers using unsupervised learning, classifying them into two categories.

GNN-Based Unsupervised Learning Solver GNN-based unsupervised learning solvers have attracted attention in CO problems [Cappart et al., 2023, Lamb et al., 2020]. Toenshoff et al. [2019], Amizadeh et al. [2018] have designed cost functions for constraint satisfaction problems, efficiently finding solutions through unsupervised learning. As previously discussed in Sec. 2.3, Schuetz et al. [2022a,b] follow a similar approach for QUBO, referred to as the PI-GNN solver. Specifically, they take the relaxed QUBO as a cost function for optimizing GNN parameters. This technique is recognized for its applicability to a wide range of practical problems and its effectiveness for large-scale CO problems. However, as discussed in Sec. 3, it is impossible to adapt to problems where the graph becomes relatively dense. On the other hand, our proposed method is capable of exploring satisfactory solutions even for the dense graph.

Machine-Learning-Assisted MCMC-Based Solver Some methods address CO problems by sampling from a corresponding Boltzmann distribution to obtain approximate solutions. Specifically, an optimization problem $\min_{\mathbf{x}} E(\mathbf{x})$ can be considered as a sampling problem from the Boltzmann distribution $p(\mathbf{x}) = e^{-\beta E(\mathbf{x})} / \sum_{\mathbf{x}} e^{-\beta E(\mathbf{x})}$, where $\sum_{\mathbf{x}}$ represents the sum over all possible states, in β infinite limit. MCMC generally performs sampling from the high-dimensional probability distribution. Recently, efforts to enhance the speed-up of MCMC methods using machine learning have garnered significant attention. Albergo et al. [2019] propose that an MCMC method accelerated by a generative model trained through the reverse-KL divergence between the target distribution and the generative model without training data. While the method can be applied to CO problems, Wu et al. [2019], Ciarella et al. [2023] implies that the method can not solve large-scale problems, and the generative models learn the complex landscape of the original cost function. In addition, McNaughton et al. [2020], Ichikawa et al. [2022] has proposed an annealing method using forward-KL divergence. Specifically, this annealing approach is training a generative model while transforming a target probability distribution from the distribution with easy sampling to with hard sampling. However, Ciarella et al. [2023] also implies that this annealing method fails in complex CO problems when using autoregressive generative models. The CRA-PI-GNN solver can find the satisfactory solutions for CO problems on relatively dense graphs at a scale of several million.

7 CONCLUSION

In this paper, we numerically demonstrate that the PI-GNN solver tends to converge to a trivial local solution, where all variables are zero, particularly in CO problems on high-degree graphs. To address this issue, we propose a new penalty term that regulates the discreteness and continuity of the relaxed variables, along with a parameter that adjusts the strength of this penalty term. In addition, this penalty term eliminates the local solution. Then, We present a continuous relaxation annealing (CRA) strategy. During the early stage of learning, the annealing is tuned for relaxed variables to favor the continuous space and eliminates the local solution, facilitating aggressive exploration in a continuous space. As learning progresses, the annealing is adjusted to make the relaxed variables favor the discrete space and then the learning terminates when the penalty term is almost zero, indicating that the relaxed variables becomes almost discrete variables, which remove the artificial transformation from continuous to discrete space Numerically, the CRA-PI-GNN solver can find reasonable solutions to CO problems on higher-degree RRGs, where the PI-GNN solver fails, and to those on relatively lower-degree RRGs with nearly the same computational time scaling. Our future endeavors include a thorough wall-clock comparison against MCMC-based solvers and greedy algorithms. Exploring specialized GNN architectures that have the comparable quality to MCMC-based solvers and faster solvers thorough transfer learning and fine-tuning remain promising future research directions.

References

- Fred Glover, Gary Kochenberger, and Yu Du. Quantum bridge analytics i: a tutorial on formulating and using qubo models. *4or*, 17:335–371, 2019.
- Gary Kochenberger, Jin-Kao Hao, Fred Glover, Mark Lewis, Zhipeng Lü, Haibo Wang, and Yang Wang. The unconstrained binary quadratic programming problem: a survey. *Journal of combinatorial optimization*, 28:58–81, 2014.
- Martin Anthony, Endre Boros, Yves Crama, and Aritanan Gruber. Quadratic reformulations of nonlinear binary optimization problems. *Mathematical Programming*, 162:115–144, 2017.
- Christos H Papadimitriou and Kenneth Steiglitz. *Combinatorial optimization: algorithms and complexity*. Courier Corporation, 1998.
- Bernhard H Korte, Jens Vygen, B Korte, and J Vygen. *Combinatorial optimization*, volume 1. Springer, 2011.
- Tameem Albash and Daniel A Lidar. Adiabatic quantum computation. *Reviews of Modern Physics*, 90(1):015002, 2018.
- Maliheh Aramon, Gili Rosenberg, Elisabetta Valiante, Toshiyuki Miyazawa, Hirotaka Tamura, and Helmut G Katzgraber. Physics-inspired optimization for quadratic unconstrained problems using a digital annealer. *Frontiers in Physics*, 7:48, 2019.
- Justin Gilmer, Samuel S Schoenholz, Patrick F Riley, Oriol Vinyals, and George E Dahl. Neural message passing for quantum chemistry. In *International conference on machine learning*, pages 1263–1272. PMLR, 2017.
- Franco Scarselli, Marco Gori, Ah Chung Tsoi, Markus Hagenbuchner, and Gabriele Monfardini. The graph neural network model. *IEEE transactions on neural networks*, 20(1):61–80, 2008.
- Martin JA Schuetz, J Kyle Brubaker, and Helmut G Katzgraber. Combinatorial optimization with physics-inspired graph neural networks. *Nature Machine Intelligence*, 4(4):367–377, 2022a.
- Martin JA Schuetz, J Kyle Brubaker, Zhihuai Zhu, and Helmut G Katzgraber. Graph coloring with physics-inspired graph neural networks. *Physical Review Research*, 4(4):043131, 2022b.
- Alan J Hoffman and Joseph B Kruskal. Integral boundary points of convex polyhedra. *50 Years of Integer Programming 1958-2008: From the Early Years to the State-of-the-Art*, pages 49–76, 2010.
- George L Nemhauser and Leslie E Trotter Jr. Properties of vertex packing and independence system polyhedra. *Mathematical programming*, 6(1):48–61, 1974.

- Maria Chiara Angelini and Federico Ricci-Tersenghi. Modern graph neural networks do worse than classical greedy algorithms in solving combinatorial optimization problems like maximum independent set. *Nature Machine Intelligence*, 5(1):29–31, 2023.
- Andrew Lucas. Ising formulations of many np problems. *Frontiers in physics*, 2:5, 2014.
- Fred Glover, Gary Kochenberger, and Yu Du. A tutorial on formulating and using qubo models. *arXiv preprint arXiv:1811.11538*, 2018.
- Richard M Karp. *Reducibility among combinatorial problems*. Springer, 2010.
- William K Hale. Frequency assignment: Theory and applications. *Proceedings of the IEEE*, 68(12):1497–1514, 1980.
- Vladimir Boginski, Sergiy Butenko, and Panos M Pardalos. Statistical analysis of financial networks. *Computational statistics & data analysis*, 48(2):431–443, 2005.
- Hristo N Djidjev, Guillaume Chapuis, Georg Hahn, and Guillaume Rizk. Efficient combinatorial optimization using quantum annealing. *arXiv preprint arXiv:1801.08653*, 2018.
- Mohsen Bayati, David Gamarnik, and Prasad Tetali. Combinatorial approach to the interpolation method and scaling limits in sparse random graphs. In *Proceedings of the forty-second ACM symposium on Theory of computing*, pages 105–114, 2010.
- Jean Barbier, Florent Krzakala, Lenka Zdeborová, and Pan Zhang. The hard-core model on random graphs revisited. In *Journal of Physics: Conference Series*, volume 473, page 012021. IOP Publishing, 2013.
- Amin Coja-Oghlan and Charilaos Efthymiou. On independent sets in random graphs. *Random Structures & Algorithms*, 47(3):436–486, 2015.
- Bahram Alidaee, Gary A Kochenberger, and Ahmad Ahmadian. 0-1 quadratic programming approach for optimum solutions of two scheduling problems. *International Journal of Systems Science*, 25(2):401–408, 1994.
- Hartmut Neven, Geordie Rose, and William G Macready. Image recognition with an adiabatic quantum computer i. mapping to quadratic unconstrained binary optimization. *arXiv preprint arXiv:0804.4457*, 2008.
- Michel Deza and Monique Laurent. Applications of cut polyhedra—ii. *Journal of Computational and Applied Mathematics*, 55(2):217–247, 1994.
- Giorgio Parisi. A sequence of approximated solutions to the sk model for spin glasses. *Journal of Physics A: Mathematical and General*, 13(4):L115, 1980.
- Amir Dembo, Andrea Montanari, and Subhabrata Sen. Extremal cuts of sparse random graphs. 2017.
- Martin JA Schuetz, J Kyle Brubaker, and Helmut G Katzgraber. Reply to: Modern graph neural networks do worse than classical greedy algorithms in solving combinatorial optimization problems like maximum independent set. *Nature Machine Intelligence*, 5(1):32–34, 2023.
- Will Hamilton, Zhitao Ying, and Jure Leskovec. Inductive representation learning on large graphs. *Advances in neural information processing systems*, 30, 2017.
- Minjie Wang, Da Zheng, Zihao Ye, Quan Gan, Mufei Li, Xiang Song, Jinjing Zhou, Chao Ma, Lingfan Yu, Yu Gai, et al. Deep graph library: A graph-centric, highly-performant package for graph neural networks. *arXiv preprint arXiv:1909.01315*, 2019.
- Diederik P Kingma and Jimmy Ba. Adam: A method for stochastic optimization. *arXiv preprint arXiv:1412.6980*, 2014.
- Maria Chiara Angelini and Federico Ricci-Tersenghi. Monte carlo algorithms are very effective in finding the largest independent set in sparse random graphs. *Physical Review E*, 100(1):013302, 2019.

- Quentin Cappart, Didier Chételat, Elias B Khalil, Andrea Lodi, Christopher Morris, and Petar Velickovic. Combinatorial optimization and reasoning with graph neural networks. *J. Mach. Learn. Res.*, 24:130–1, 2023.
- Luís C Lamb, Artur Garcez, Marco Gori, Marcelo Prates, Pedro Avelar, and Moshe Vardi. Graph neural networks meet neural-symbolic computing: A survey and perspective. *arXiv preprint arXiv:2003.00330*, 2020.
- Jan Toenshoff, Martin Ritzert, Hinrikus Wolf, and Martin Grohe. Run-csp: unsupervised learning of message passing networks for binary constraint satisfaction problems. *CoRR, abs/1909.08387*, 2019.
- Saeed Amizadeh, Sergiy Matuselych, and Markus Weimer. Learning to solve circuit-sat: An unsupervised differentiable approach. In *International Conference on Learning Representations*, 2018.
- Michael S Albergo, Gurtej Kanwar, and Phiala E Shanahan. Flow-based generative models for markov chain monte carlo in lattice field theory. *Physical Review D*, 100(3):034515, 2019.
- Dian Wu, Lei Wang, and Pan Zhang. Solving statistical mechanics using variational autoregressive networks. *Physical review letters*, 122(8):080602, 2019.
- Simone Ciarella, Jeanne Trinquier, Martin Weigt, and Francesco Zamponi. Machine-learning-assisted monte carlo fails at sampling computationally hard problems. *Machine Learning: Science and Technology*, 4(1):010501, 2023.
- B McNaughton, MV Milošević, A Perali, and S Pilati. Boosting monte carlo simulations of spin glasses using autoregressive neural networks. *Physical Review E*, 101(5):053312, 2020.
- Yuma Ichikawa, Akira Nakagawa, Hiromoto Masayuki, and Yuhei Umeda. Toward unlimited self-learning monte carlo with annealing process using vae’s implicit isometricity. *arXiv preprint arXiv:2211.14024*, 2022.

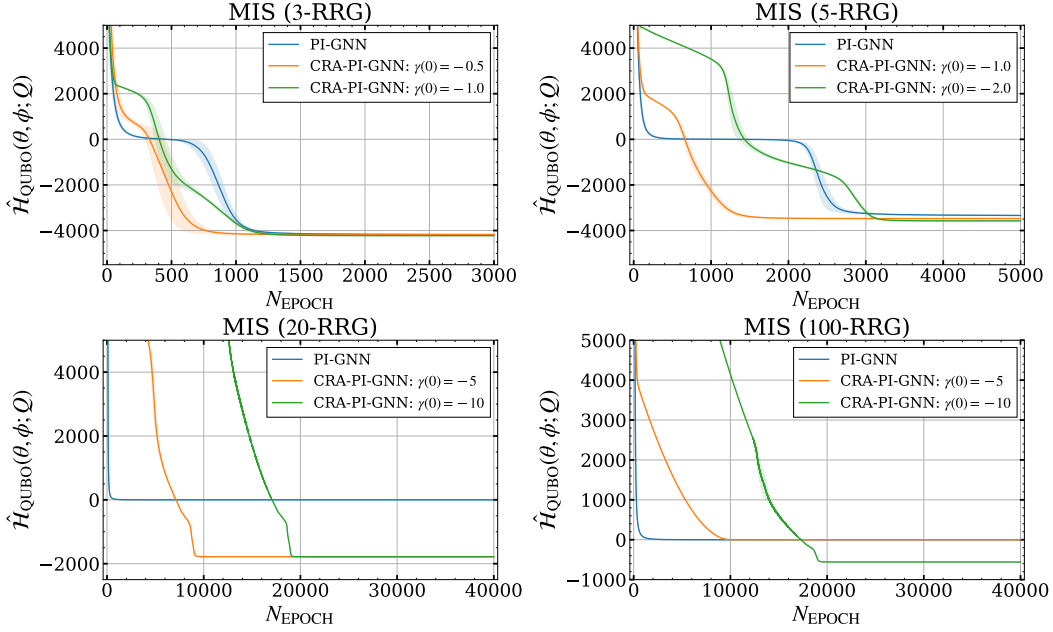


Figure 5: The cost function of $N = 10000$ MIS problems on RRGs of varying degrees d as a function of the number of parameters updates, N_{EPOCH} . The lines represent the average cost function over five different instances, and the shade corresponding to each line represents the standard deviation of the results.

A ADDITIONAL EXPERIMENTS

A.1 Dynamics of Cost Functions

This section demonstrates how the CRA-PI-GNN solver quickly escapes from the local solution where all relaxed variables are zero. Using the GCV with the same settings as in Sec. 5.1, we solved MIS problems on RRGs of various degrees with $N = 10000$. Fig. 5 shows the cost functions of the MIS problems on RRGs with $N = 10000$ and $d = 3, 5, 20, 100$ as functions of N_{EPOCH} . For RRG with $d = 3, 5$, the CRA-PI-GNN solver can easily escape from the plateau, $\hat{H}(\theta, \phi; Q) = 0$ and then find a better solution with fewer epochs N_{EPOCH} . Furthermore, while the PI-GNN solver struggles to escape from the plateau for $d = 20, 100$, the figure shows that the CRA-PI-GNN solvers can escape from the plateau and then find a satisfactory solution.

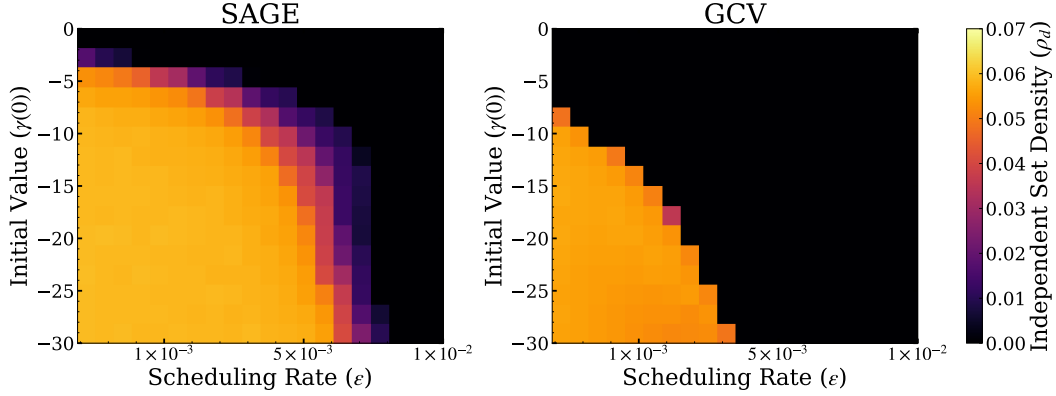


Figure 6: (Top) Independent set density of $N = 10000$ MIS problems on 100-RRG as a function of initial scheduling value $\gamma(0)$ and scheduling rate ϵ obtained by the CRA-PI-GNN solver using GraphSage (Left) and GCV (Right). The heat map color represents the average independent set over five different instances.

A.2 Ablation over Initial Scheduling Value and Scheduling Rate

We conducted an ablation study focusing on initial scheduling value $\gamma(0)$ and scheduling rate ϵ . The numerical experiment was conducted under the same configuration as in Sec. 5.1. Fig. 6 presents the independent set density of $N = 10000$ MIS problems on 100-RRG as a function of the initial scheduling value $\gamma(0)$ and the scheduling rate ϵ using the CRA-PI-GNN with GraphSage and GCV. As shown in Fig. 6, we observe that smaller initial scheduling value $\gamma(0)$ and scheduling rate ϵ typically yield better solutions. However, note that as initial scheduling value $\gamma(0)$ and scheduling rate ϵ are smaller, convergence time gets progressively longer. In addition, GraphSage consistently produces better solutions even with a relatively larger initial scheduling value $\gamma(0)$ and scheduling rate ϵ . This implies that GNN architecture influences not only the quality of the solution but also the effective regions of initial scheduling value $\gamma(0)$ and scheduling rate ϵ for the annealing.